Supplementary Information (SI) for Energy & Environmental Science.

Halogenated polystyrene derivatives passivate and prevent volatilization in inverted perovskite solar cells

*Saikiran. S. Khamgaonkar and Vivek Maheshwari**

S.S. Khamgaonkar and V. Maheshwari

Department of Chemistry

Waterloo Institute for Nanotechnology

200 University Ave. West Waterloo, ON N2L 3G1, Canada

E-mail: vmaheshw@uwaterloo.ca

1. Materials

The pre-patterned fluorine-doped tin oxide (FTO) substrate with 8 ohms sq^{-1} resistance was purchased from Ying Kou Shangsheng Co Ltd. Formamidinium iodide (FAI), methylammonium bromide (MABr) and methylammonium chloride (MACl), were purchased from Great Cell Solar Materials. (2-(3,6-dimethoxy-9 H-carbazol-9-yl)ethyl)phosphonic acid (MeO-2PACz) and lead bromide ($PbBr_2$) were purchased from TCI America. Dimethyl formamide (DMF), dimethyl sulfoxide (DMSO), isopropyl alcohol (IPA), anisole, chlorobenzene, cesium iodide (CsI), and lead iodide (PbI_2), were purchased from Sigma-Aldrich. C_{60} and bathocuproine (BCP) were purchased from Ossila. Different halogenated polystyrene, (PS), polymer 4-bromopolystyrene (PS-Br), 4-fluoropolystyrene (PS-F), 4-chloropolystyrene (PS-Cl), and pentafluoro polystyrene (PFS) were purchased from Polymer Source Inc. Encapsulation cover glass and UV curing glue were purchased from Luminescence Technology Corp.

2. Perovskite Precursor Solution Preparation

a) $Cs_{0.05}FA_{0.9}MA_{0.05}Pb(Br_{0.05}I_{0.95})$

1.45 M $Cs_{0.05}FA_{0.9}MA_{0.05}Pb(Br_{0.05}I_{0.95})_3$ solution was prepared by dissolving 0.0725 mmol CsI, 0.0725 mmol of MABr, 1.305 mmol FAI, 0.0725 mmol $PbBr_2$, and 1.38 mmol PbI_2 in 1 mL mixture of DMF and DMSO (4:1 by volume). 10 mg mL^{-1} of MACl was added to the solution to improve the quality and crystallization of perovskite thin films.

b) $Cs_{0.05}$ $FA_{0.95}PbI_3$

1.45M $Cs_{0.05}FA_{0.95}PbI_3$ was prepared by mixing FAI, CsI and PbI_2 with a molar ratio of 0.95:0.05:1 in 1ml of mixture of DMF and DMSO (4:1 by volume).

c) $MAPbI_3$

1.45M $MAPbI_3$ perovskite solution was prepared by mixing PbI_2 and MAI in 1:1 molar ratio in 1ml of mixture of DMF and DMSO (6:1 by volume).

Further all the precursor solution was stirred at 60 °C for 2 h and then filtered using a 0.22 um polytetrafluoroethylene (PTFE) membrane before use. For bulk passivation by individual halogenated PS derivatives, an optimized 1 wt% of respective polymers was first dissolved and mixed well in a DMF/DMSO mixture solution. This polymer-dissolved DMF/DMSO solution was then used as the solvent for dissolving the perovskite precursor. After complete dissolution of the perovskite precursors, a gel of polymer can be seen inside the solution, this indicates the cross-linking of polymer in the solution. For top perovskite/ETL polymer passivation, respective polymers were dissolved in chlorobenzene with an optimized concentration of 2 mg mL^{-1} .

3. Device Fabrication

Prepatterned fluorine-doped tin oxide (FTO) glasses were cleaned using Millipore water, acetone, and isopropanol each for 15 min in an ultrasonic bath, followed by ultraviolet ozone treatment for 25 min. The HTL was prepared by dissolving using 0.5 mg mL^{-1} MeO-2PACz powder in IPA. The MeO-2PACz in IPA solution was spin-coated on FTO at 3500 rpm. for 30 s, followed by annealing at 110 °C for 10 min. The perovskite precursor solution with and without the addition of polymers was prepared according to the procedure given above. The perovskite solutions were spin-coated at 1000 rpm for 6 s and 5500 rpm. for 24 s respectively. At the last 10 s of the second step, 70 µL anisole was dropped as an antisolvent. The films were then annealed at 110 °C for 20 mins. For perovskite top passivation, respective polymer solution 2 mg mL^{-1} in chlorobenzene was spin-coated at 5500 rpm for 30 s and then annealed at 100 °C for 10 mins. A 25nm thick ETL layer of C_{60} was thermally evaporated at a rate of 0.25A/s, followed by thermal evaporation of a 7nm thin BCP interfacial layer at a rate of 0.15A/s. Finally, to complete the device 100 nm of thick silver electrodes were thermally evaporated.

4. Characterization

^{1}HNMR analysis of various perovskite precursors was performed on Bruker-300 Ultra shield NMR instrument. The topspin NMR software was used to analyze the NMR spectrum. The XPS characterization of perovskite thin films was performed on the VGS ESCA Lab 250 instrument. The XPS spectrum was calibrated in Casa XPS software using the C 1s peak, setting the C–C (adventitious carbon) component to 284.8 eV. The depth profiles of freshly prepared perovskite films on Si substrates were analyzed using TOF–SIMS (IONTOF M5 instrument) by employing a Cs^+ ion source (500 eV) for sputtering and Bi^{3+} (30 eV) for analysis. Grazing incidence XRD measurements were performed using a PANalytical X'Pert Pro MRD diffractometer with Cu Kα radiation ($\lambda = 1.54$ Å) at an incidence angle of 0.6°. A Zeiss ultra plus field-emission scanning electron microscopy (FESEM) was used to measure the morphology of the perovskite thin films. The electrical measurement on the lateral device configuration of the Au/perovskite /Au was conducted using a two-probe station. A Keysight 6614C 50-watt power system supply was used for applying an external bias. The current response was recorded using Keysight 3458 A Digital multimeter. UPS measurements were performed on the Nexsa G2 Surface Analysis System under the excitation of the He 1 line (21.22eV) of a helium discharge lamp. The optical absorption spectra were recorded using a UV-visible spectrophotometer (Perkin Elmer Lambda 750). High-temperature XRD diffraction patterns for polymer-perovskite thin films were obtained from a Malvern Panalytical X-ray diffractometer operated under inert Ar conditions. For TGA analysis, samples were prepared by spin-coating perovskite thin films, followed by carefully scraping the powder off the film using a blade. TGA analysis was done under Ar conditions using an SDT-Q600 Simultaneous TGA / DSC analyzer. For determining the contact angle and the average grain size, Image J software was used.

5. Device Testing

The *J–V* characteristics were measured using an Ivium Technologies Potentiostat under illumination from a Xenon-lamp-based solar simulator (Newport Oriel Instrument, 450 W Solar Simulator) with a light intensity of 100 mW cm^{-2}. The light intensity was calibrated to 100 mW cm^{-2} using an NREL-calibrated KG5 silicon reference cell. The active area of the solar cell is 0.1695 cm^{-2}. The *J–V* curves were measured at a scan rate of 100 mV s^{-1} with a potential step of 10 mV. The *J–V* hysteresis characteristics were measured by running continuously ten *J–V* sweeps at a slow scan rate of 100 mV s^{-1}. All the device testing was done in ambient conditions. The hysteresis index of the devices was calculated by the equation Hysteresis index = $|(PCE_{reverse} - PCE_{forward})/PCE_{reverse}|$.

6. Stability Testing

For stability testing the devices were encapsulated with a cover glass encapsulant with edge sealing by a UV-curable glue (Lumtec LT-U001). The ISOS D-1 and D-2 dark storage testing was performed by keeping the encapsulated devices in the dark under ambient conditions for D-1 and at 65 °C in the oven for D-2. The device performance was evaluated periodically under ambient conditions. The MPP tracking was performed under ambient conditions under continuous illumination. For MPP tracking periodic J-V curves were performed, and according to J-V analysis the cells were held at the maximum power point voltage to get the output maximum power.

7. First-principle calculations

The calculations for the dipole moment and charge distribution of individual monomers were performed using Gaussian 16 with the B3LYP method. The geometries of individual monomers were optimized using Avogadro software. For ESP maps of individual monomers Gauss view software was used.

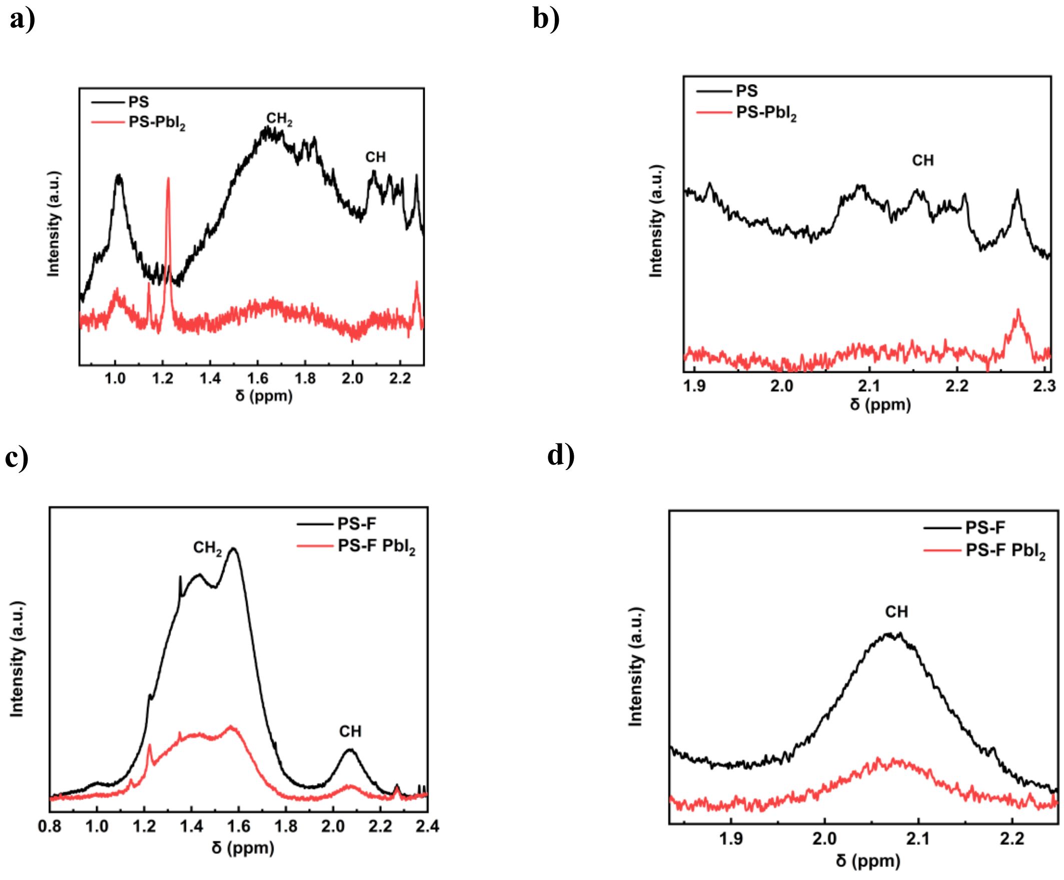

Fig S1. **a, c)** ^{1}HNMR spectrum of aliphatic regions of PS, PS-F pristine polymers and polymers dissolved in PbI$_2$ **b, d)** Zoom in backbone CH proton region for both the polymers.

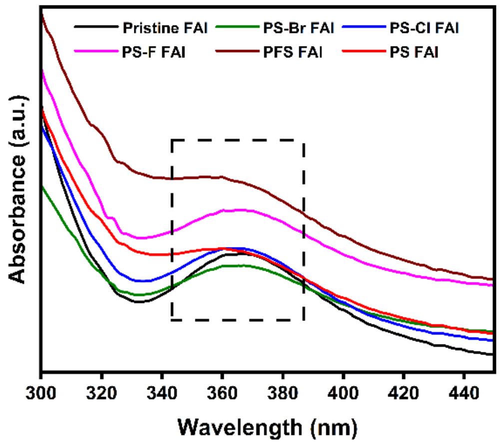

Fig S2. UV- visible spectrum of pristine FAI and polymer-FAI solutions, dissolved in DMF/DMSO solution. The square rectangular box represents the peak due to the presence of I^- or I_3^- species in FAI.

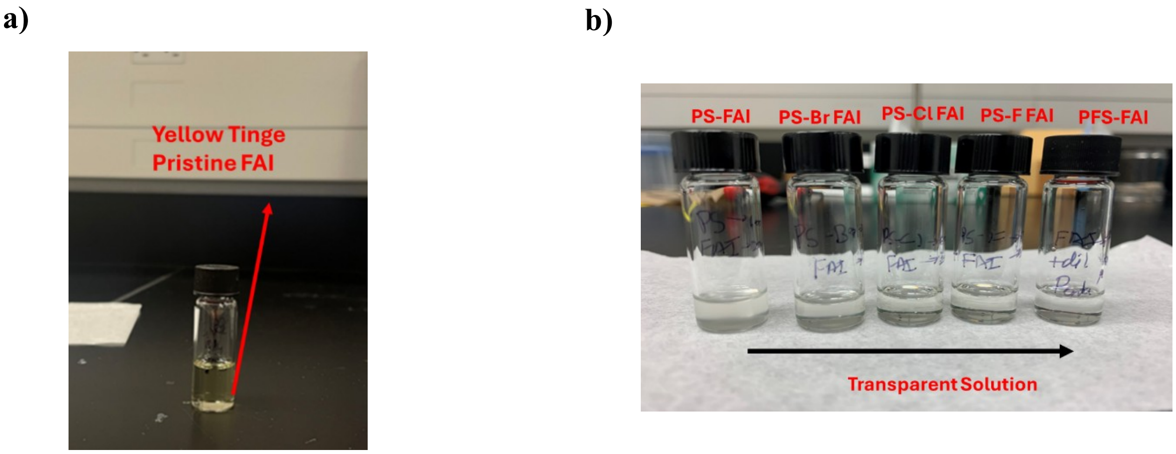

Fig S3. a) Photograph of yellow colored FAI solution dissolved in DMF/DMSO solution. **b)** Photographs of various polymers (PS at left most followed by PS-Br, PS-Cl, PS-F and PFS) mixed FAI solutions showing much more transparency when compared to plain FAI solution.

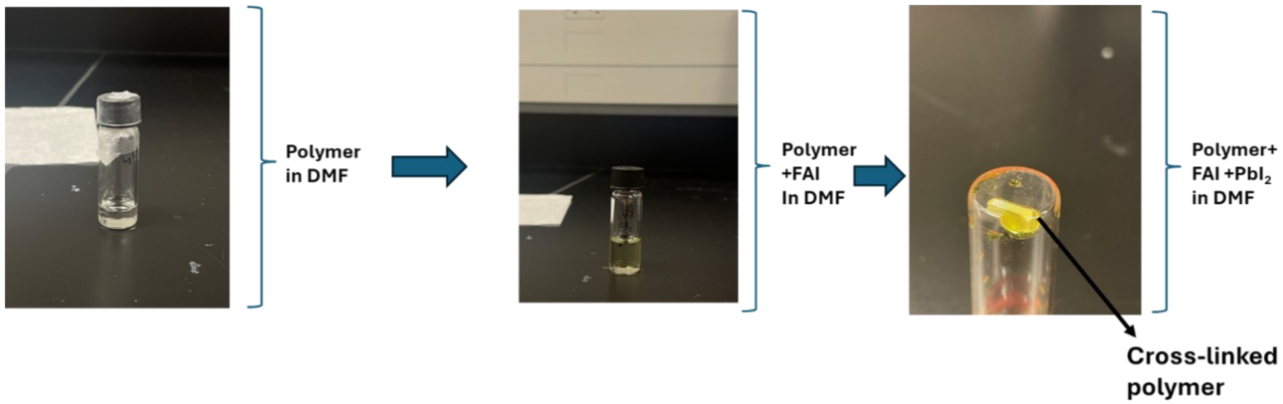

Fig S4. Photographs at various stages of mixing of polymer in perovskite precursor. Initially, individual polymers were dissolved in DMF. Then in the dissolved polymer solution FAI was further dissolved, leading to the formation of homogenously dissolved precursor solution. At the end PbI_2 was dissolved by continuously stirring the solution at 60 °C. After the complete dissolution of PbI_2 a gel was formed in the case of all the five polymers. This confirmed the crosslinking of the polymer chains due to the presence of PbI_2.

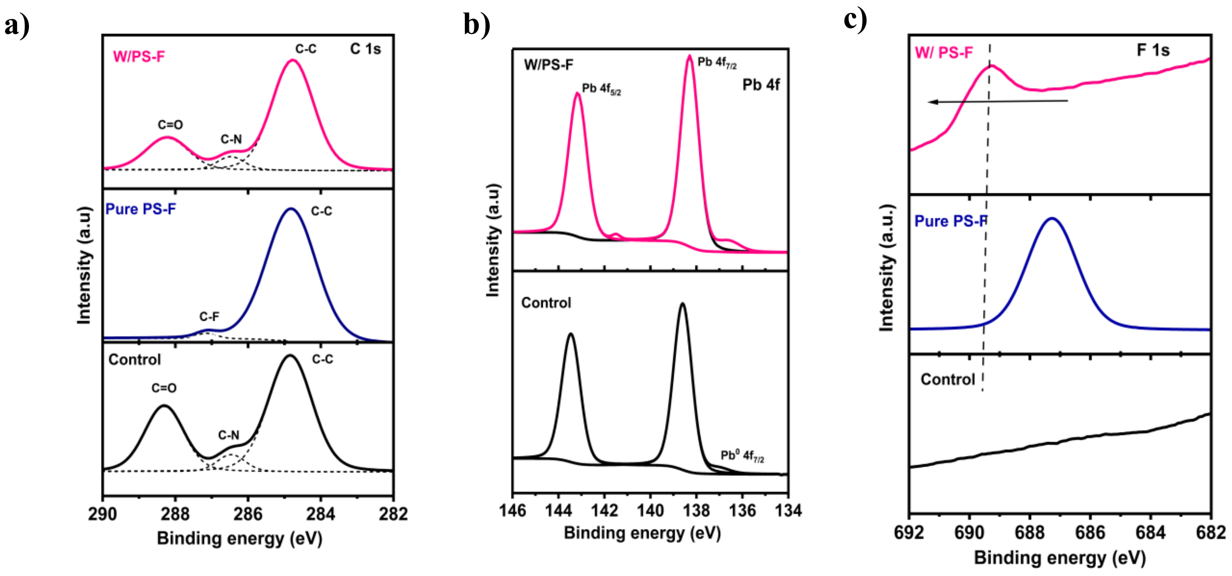

Fig S5 a, c) High resolution C1s and F1s XPS spectrum for pure PS-F polymer, control and PS-F incorporated perovskite thin films. **b)** High resolution Pb 4f XPS spectrum of control and PS-F incorporated perovskite thin films.

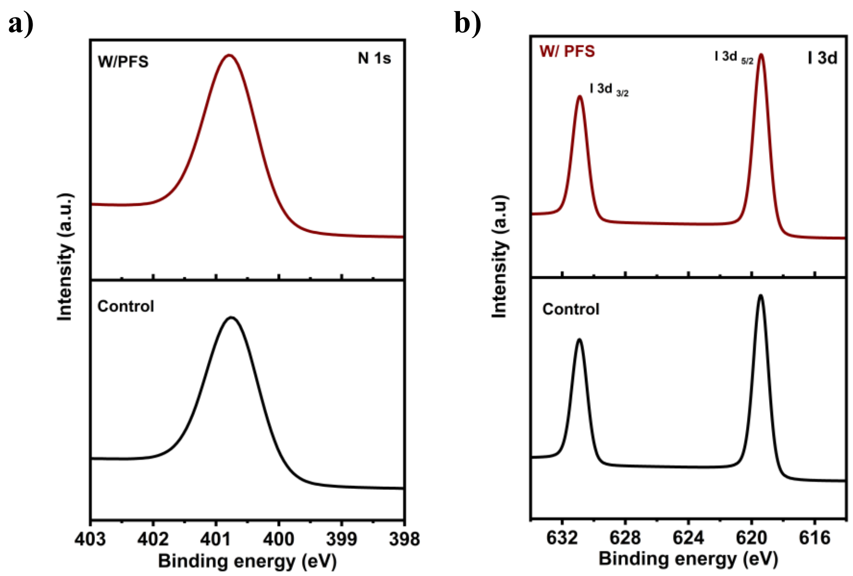

Fig S6 a, b) High resolution N1s and I 3d XPS spectrum for control and PFS incorporated perovskite thin films.

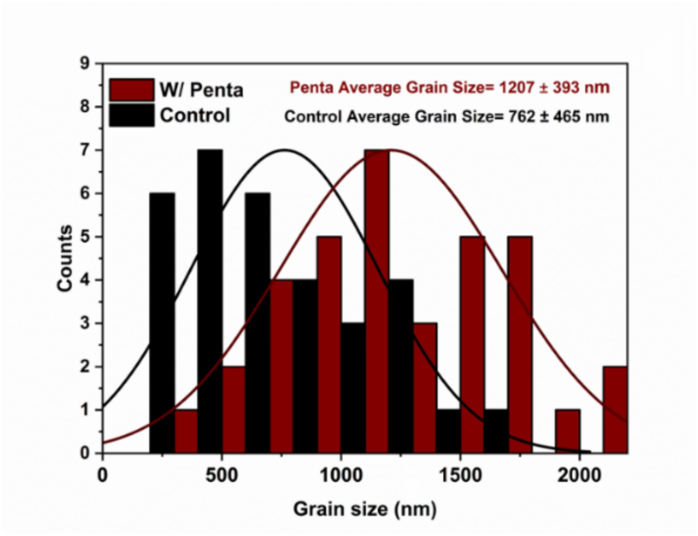

Fig S 7. Statistical average grain size distribution plots for control and PFS modified perovskite thin films.

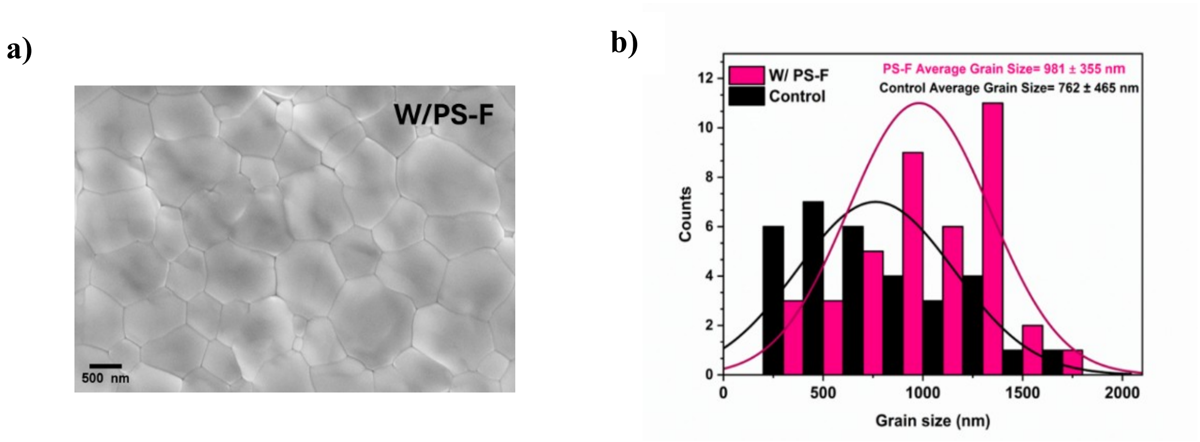

Fig S 8 a) Top view SEM image of PS-F modified perovskite thin films. **b)** Statistical average grain size distribution plots for control and PS-F modified perovskite thin films.

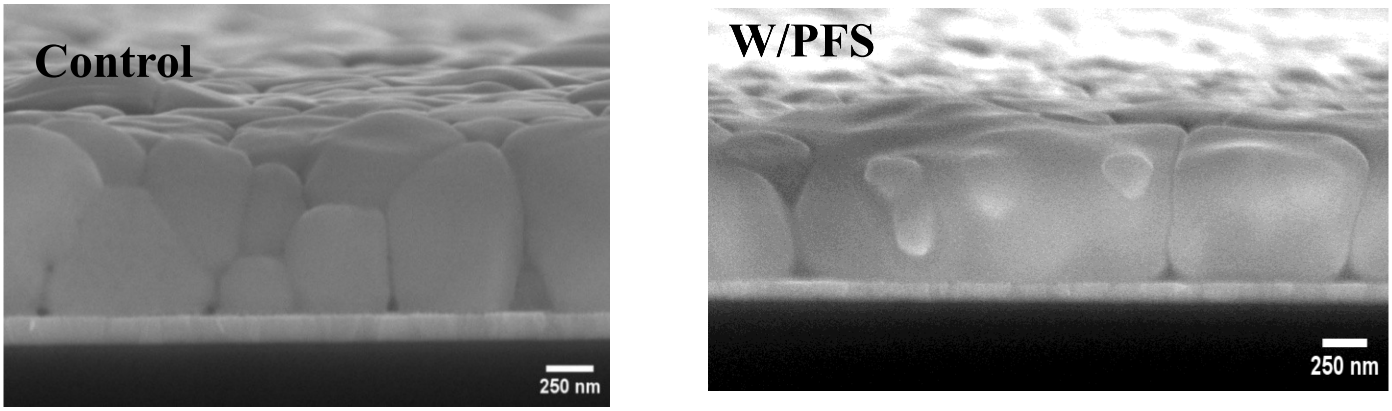

Fig S 9. Cross sectional SEM images for control and PFS modified perovskite thin films.

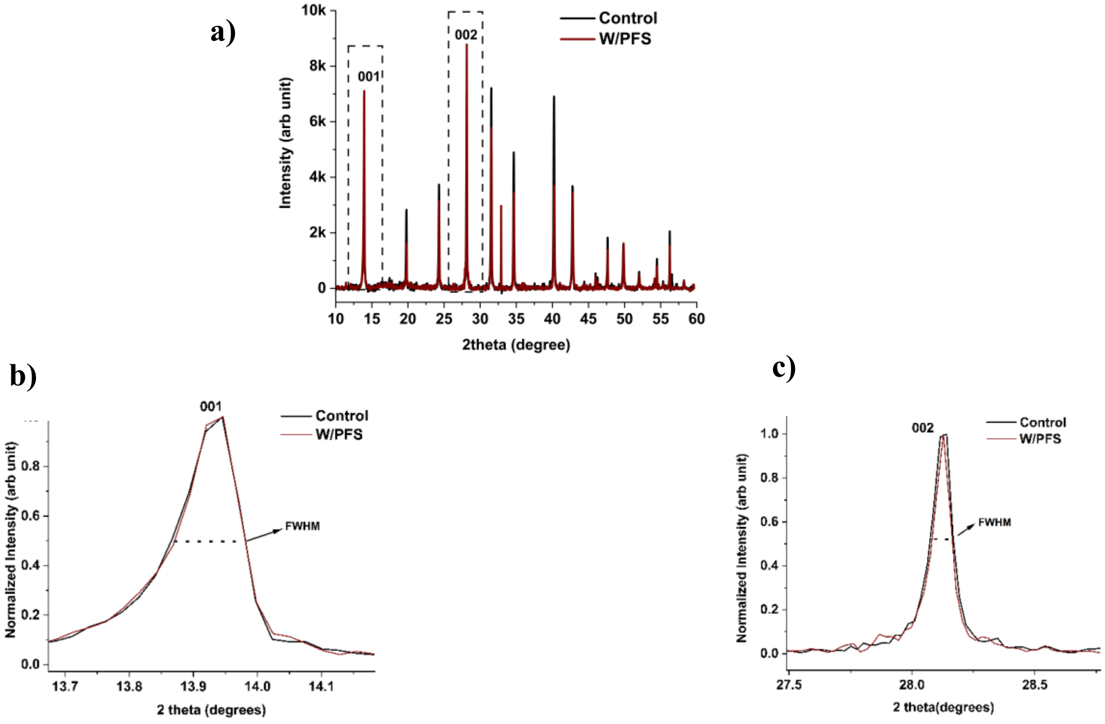

Fig S 10. **a)** XRD powder diffraction pattern for control and PFS passivated perovskite thin films **b** and **c)** Zoom in XRD patterns for 001 and 002 peaks. A narrowing in FWHM is observed in case in PFS incorporated perovskite thin films indicated by dashed lines when compared to control thin films.

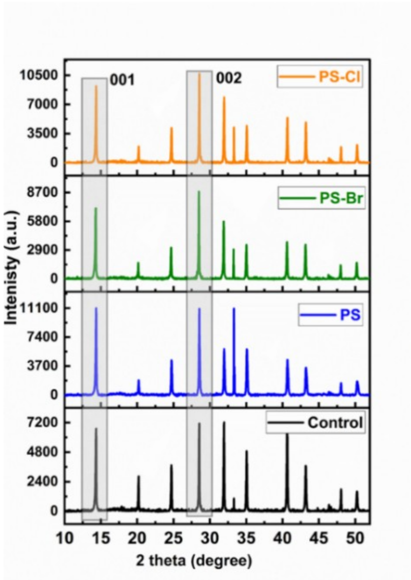

Fig S 11. Powder X-ray diffraction patterns for control, PS, PS-Br, PS-Cl polymer-perovskite thin films. the rectangular shaded region indicates the major 001 and 002 peaks.

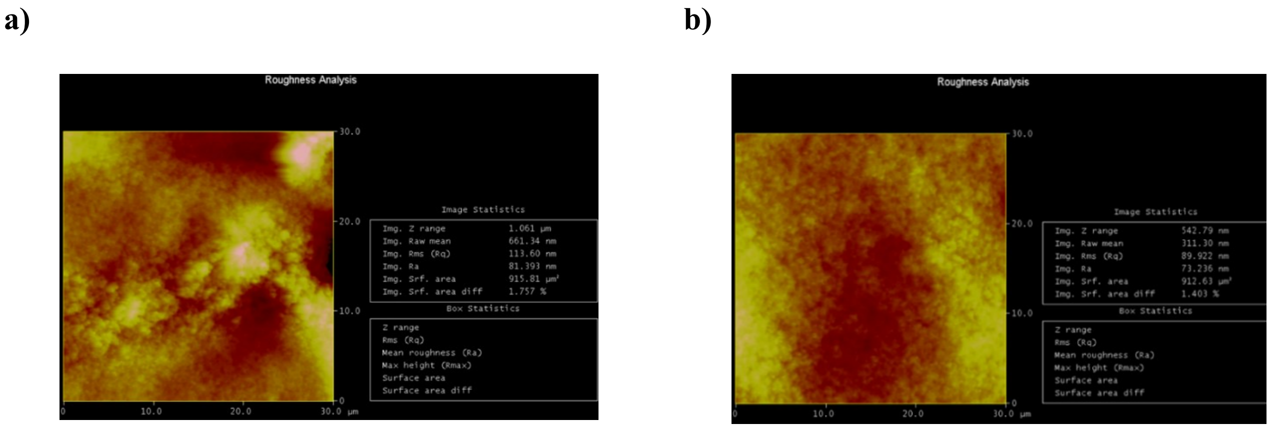

a)

Image Statistics

Img. Z range	1.061 µm
Img. Raw mean	661.34 nm
Img. Rms (Rq)	113.60 nm
Img. Ra	81.393 nm
Img. Srf. area	915.81 µm²
Img. Srf. area diff	1.757 %

Box Statistics

Z range
Rms (Rq)
Mean roughness (Ra)
Max height (Rmax)
Surface area
Surface area diff

b)

Image Statistics

Img. Z range	542.79 nm
Img. Raw mean	311.30 nm
Img. Rms (Rq)	89.922 nm
Img. Ra	73.236 nm
Img. Srf. area	912.63 µm²
Img. Srf. area diff	1.403 %

Box Statistics

Z range
Rms (Rq)
Mean roughness (Ra)
Max height (Rmax)
Surface area
Surface area diff

Fig S12 a, b). AFM images of 30*30 µm area of control and PFS modified perovskite thin films.

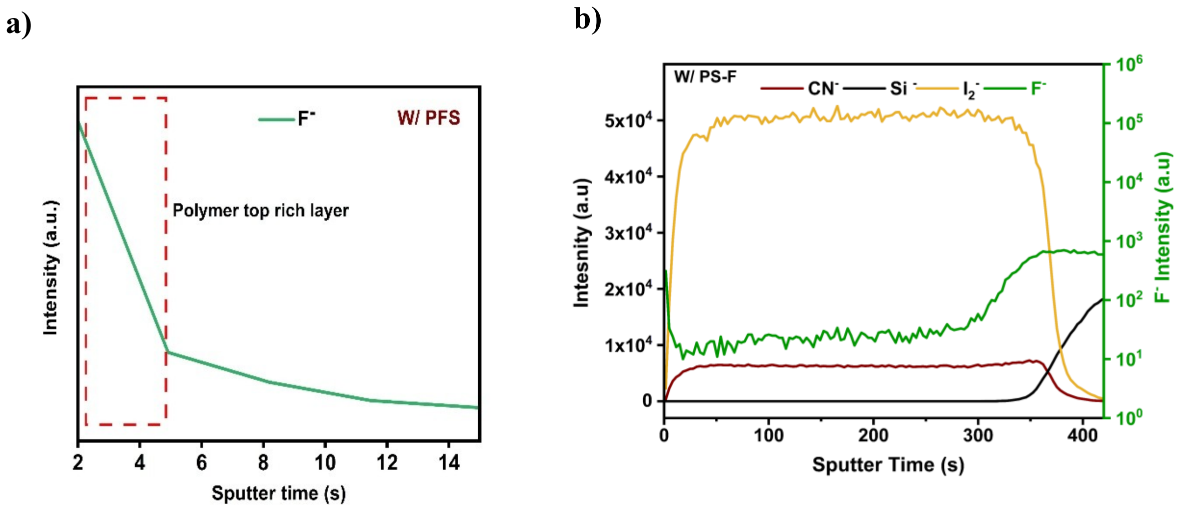

Fig S13 a) Zoom in F^- TOF-SIMs spectrum for PFS polymer perovskite thin films, showing a fluorine rich top interface during 10s of sputtering. **b)** TOF-SIMS depth profile of PS-F incorporated perovskite thin films. For clarity and ease of identification, the F^- signal (green color) in Figure 13 **b** is plotted on secondary y axis in log scale.

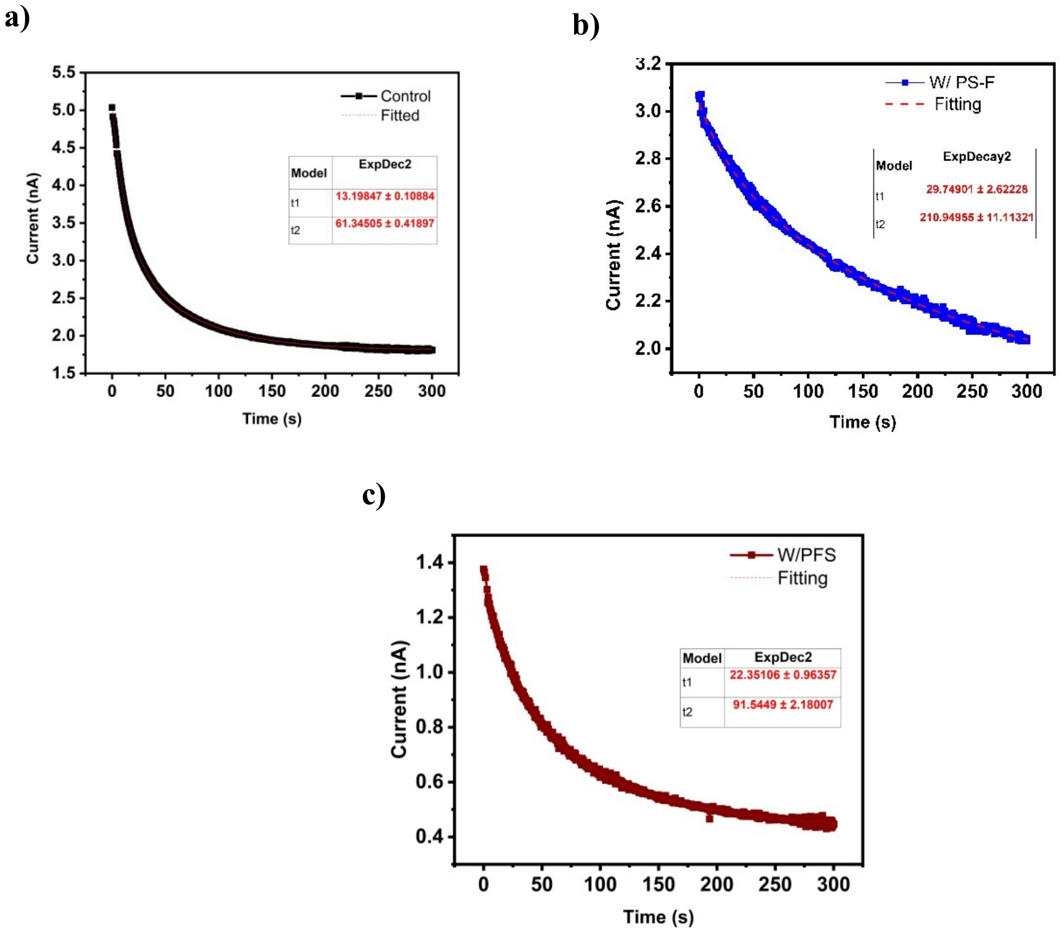

Fig S14 a, b, c) Dark poling curve for control, PS-F and PFS incorporated perovskite thin films fitted with a biexponential decay function. The inset table shows the t_1 and t_2 biexponential fitted, decay time constants.

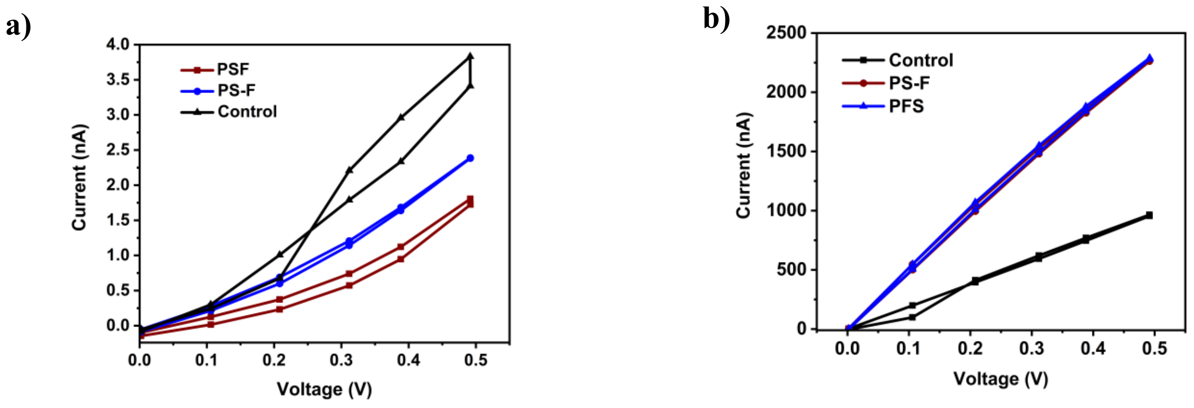

Fig S15 a, b) Dark and light I-V curves for lateral Au| $Cs_{0.05}$ $FA_{0.9}$ $MA_{0.05}$ Pb $(I_{0.95}Br_{0.05})_3$ |Au device with control, PS-F and PFS incorporated polymer perovskite thin films.

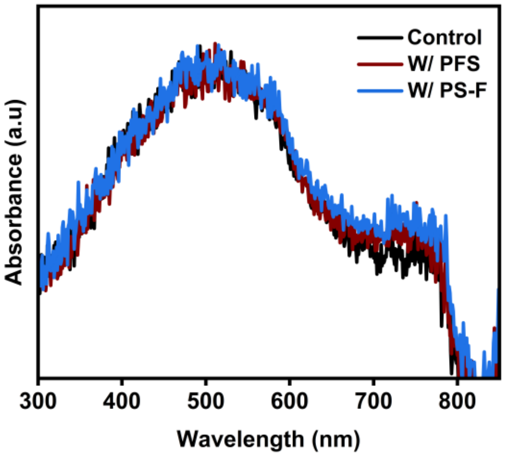

Fig S16 UV-vis spectrum for control, PS-F and PFS polymer perovskite thin films. No change in absorption characteristics is seen indicating a unchanged band gap due to the incorporation of polymer.

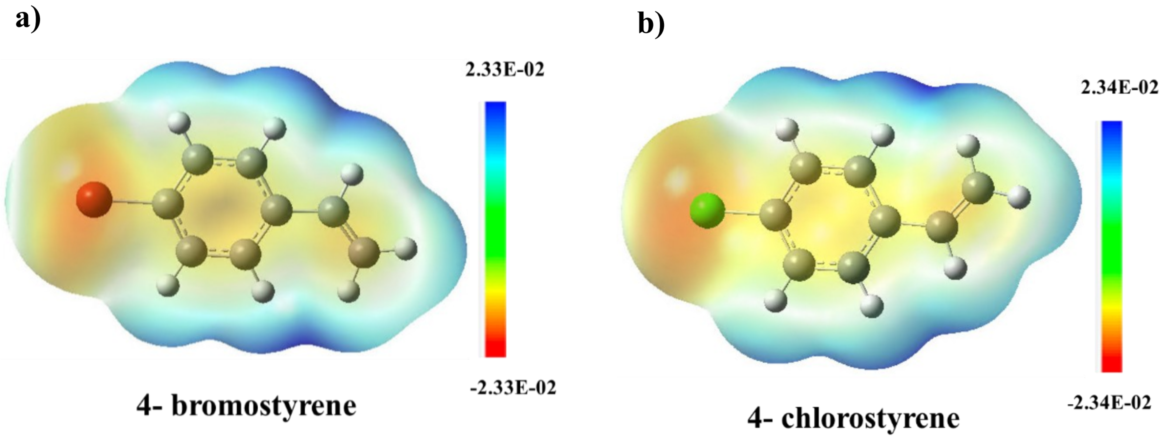

Fig S17 a, b ESP profiles for 4-bromostyrene and 4-chlorostyrene monomer. The red sphere represents Br atom while the green sphere represents the chlorine atom.

a)

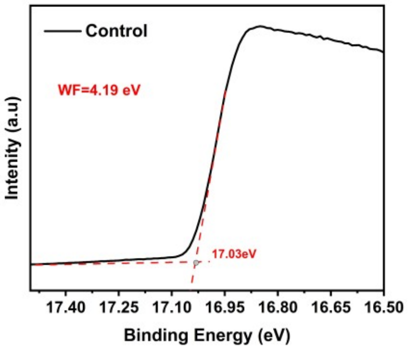

Control
WF=4.19 eV
17.03eV
Intenity (a.u)
17.40
17.25
17.10
16.95
16.80
16.65
16.50
Binding Energy (eV)

b)

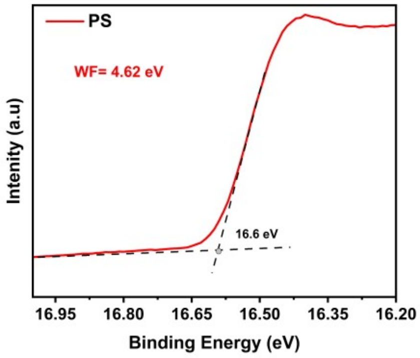

PS
WF= 4.62 eV
16.6 eV
Intenity (a.u)
16.95
16.80
16.65
16.50
16.35
16.20
Binding Energy (eV)

c)

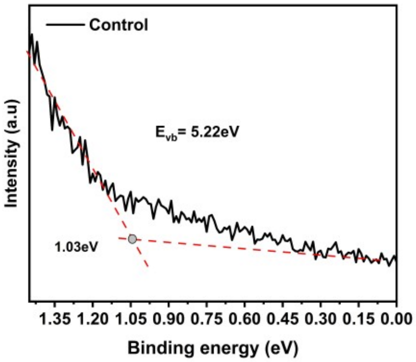

Control
E_{vb}= 5.22eV
1.03eV
Intensity (a.u)
1.35
1.20
1.05
0.90
0.75
0.60
0.45
0.30
0.15
0.00
Binding energy (eV)

d)

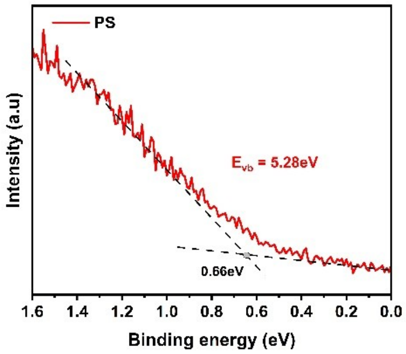

PS
E_{vb} = 5.28eV
0.66eV
Intensity (a.u)
1.6
1.4
1.2
1.0
0.8
0.6
0.4
0.2
0.0
Binding energy (eV)

e)

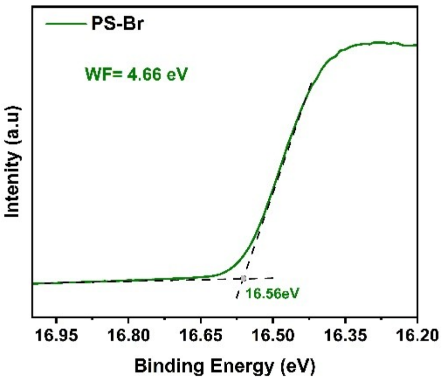

PS-Br
WF= 4.66 eV
16.56eV
Intenity (a.u)
16.95
16.80
16.65
16.50
16.35
16.20
Binding Energy (eV)

f)

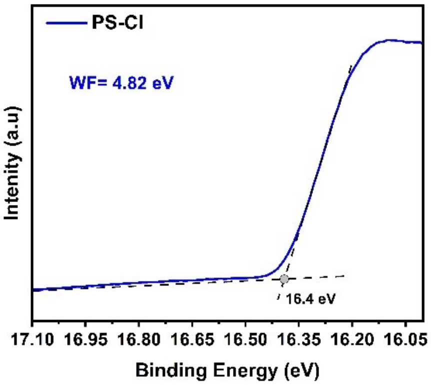

PS-Cl
WF= 4.82 eV
16.4 eV
Intenity (a.u)
17.10
16.95
16.80
16.65
16.50
16.35
16.20
16.05
Binding Energy (eV)

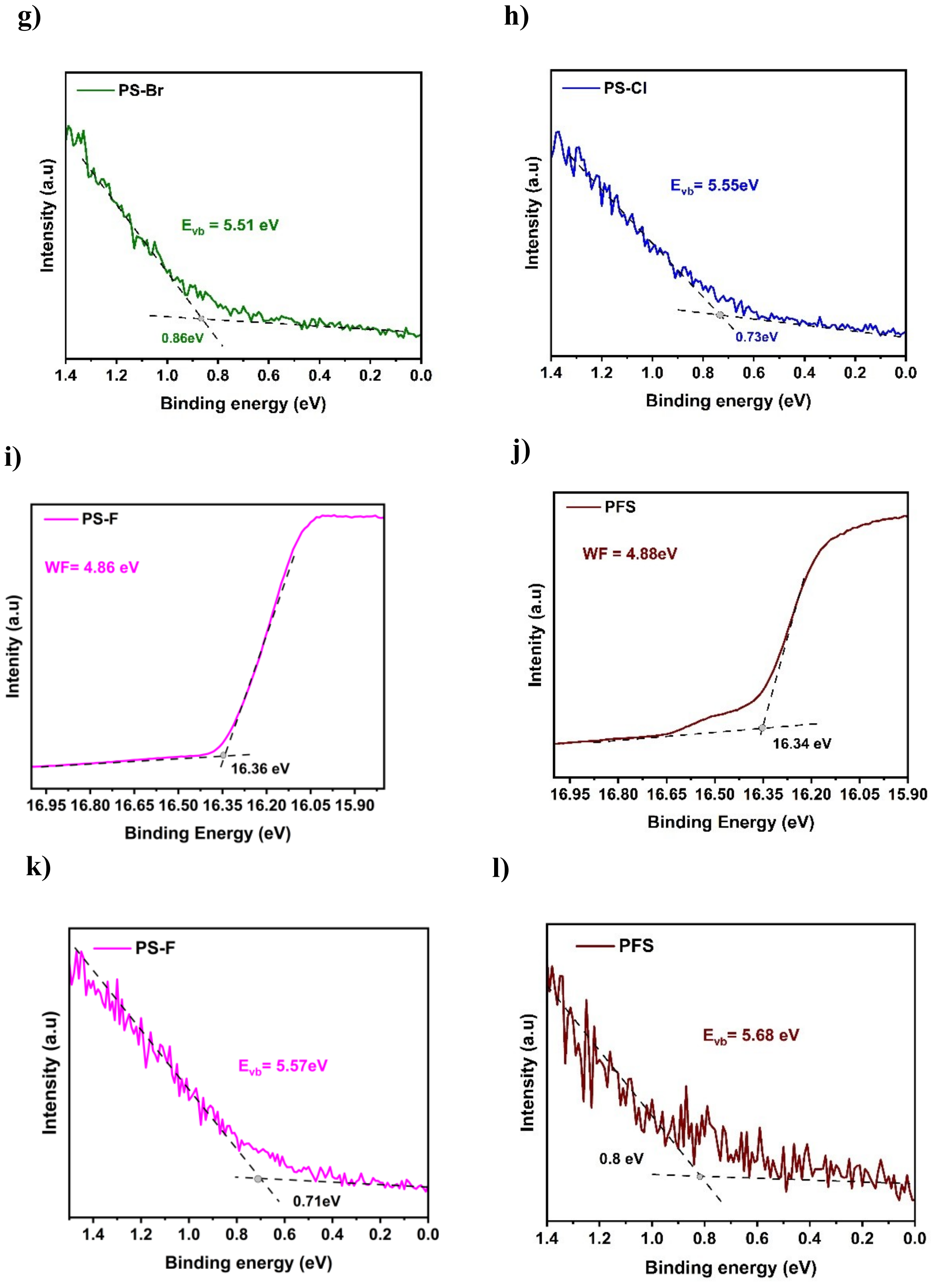

Fig S18 a, b, e, f, i, j Secondar electron cut off region to determine work function for control, PS, PS-Br, PS-Cl, PS-F and PFS incoproated perovskite thin films. **c, d, g, h, k, l** Valence band onset region for control, PS, PS-br, PS-Cl, PS-F and PFS used to calacute the valence band.

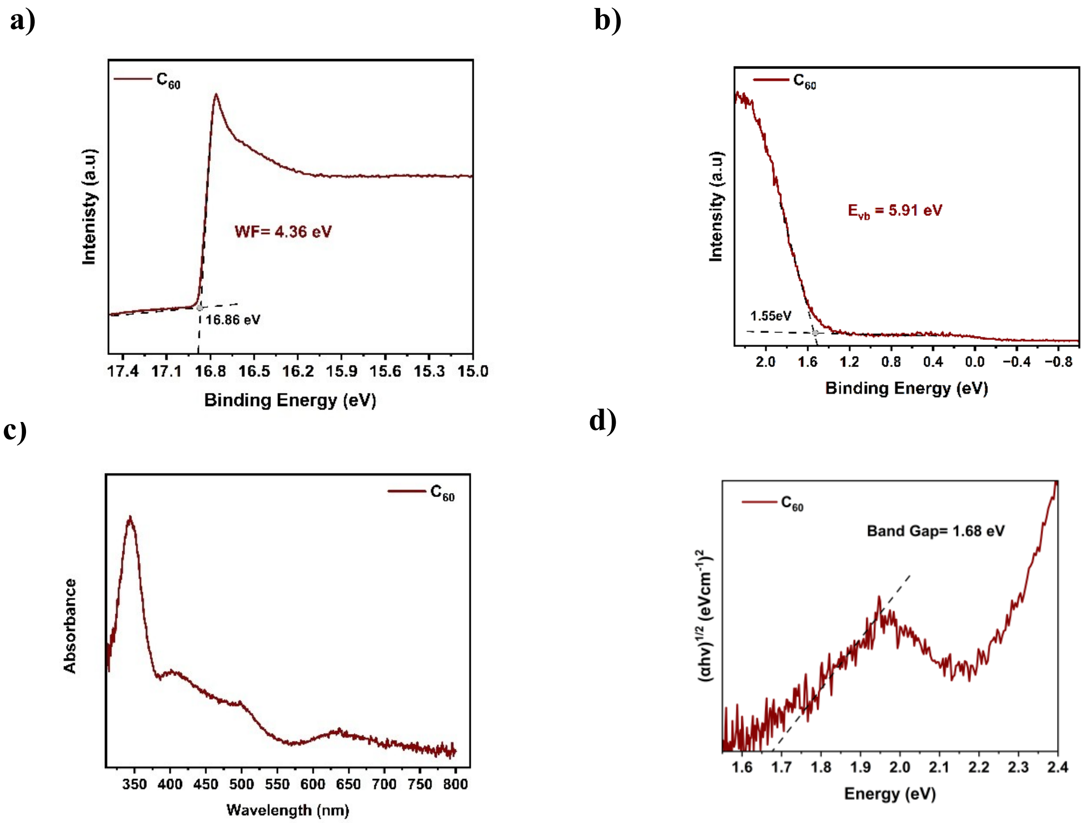

Fig S19 a, b) Secondary electron cutoff region and valence band region for pure C$_{60}$ thin film. **c, d)** Absorption spectrum and Tauc plot for C$_{60}$ thin films.

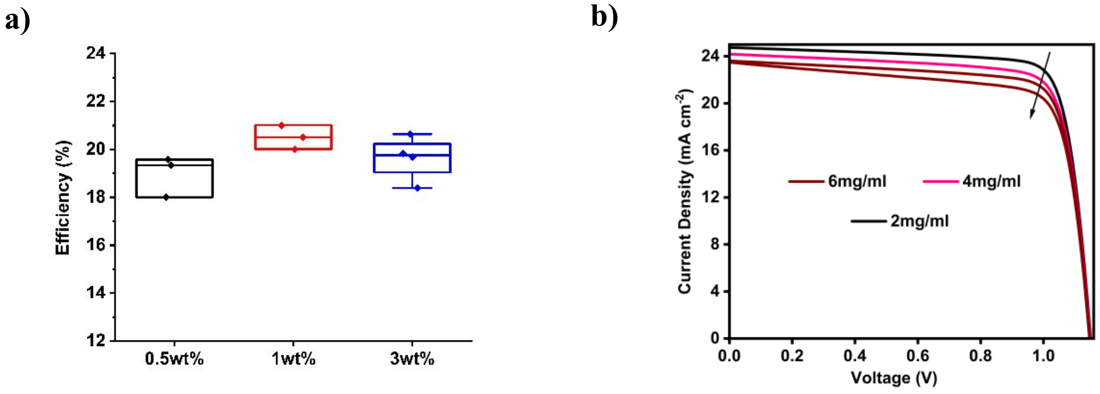

Fig S20 a) Effect of varying concentration of polymer inside the perovskite precursor for effective perovskite bulk passivation. **b)** Effect of varying polymer top interlayer concentrations on the performance of perovskite solar cells.

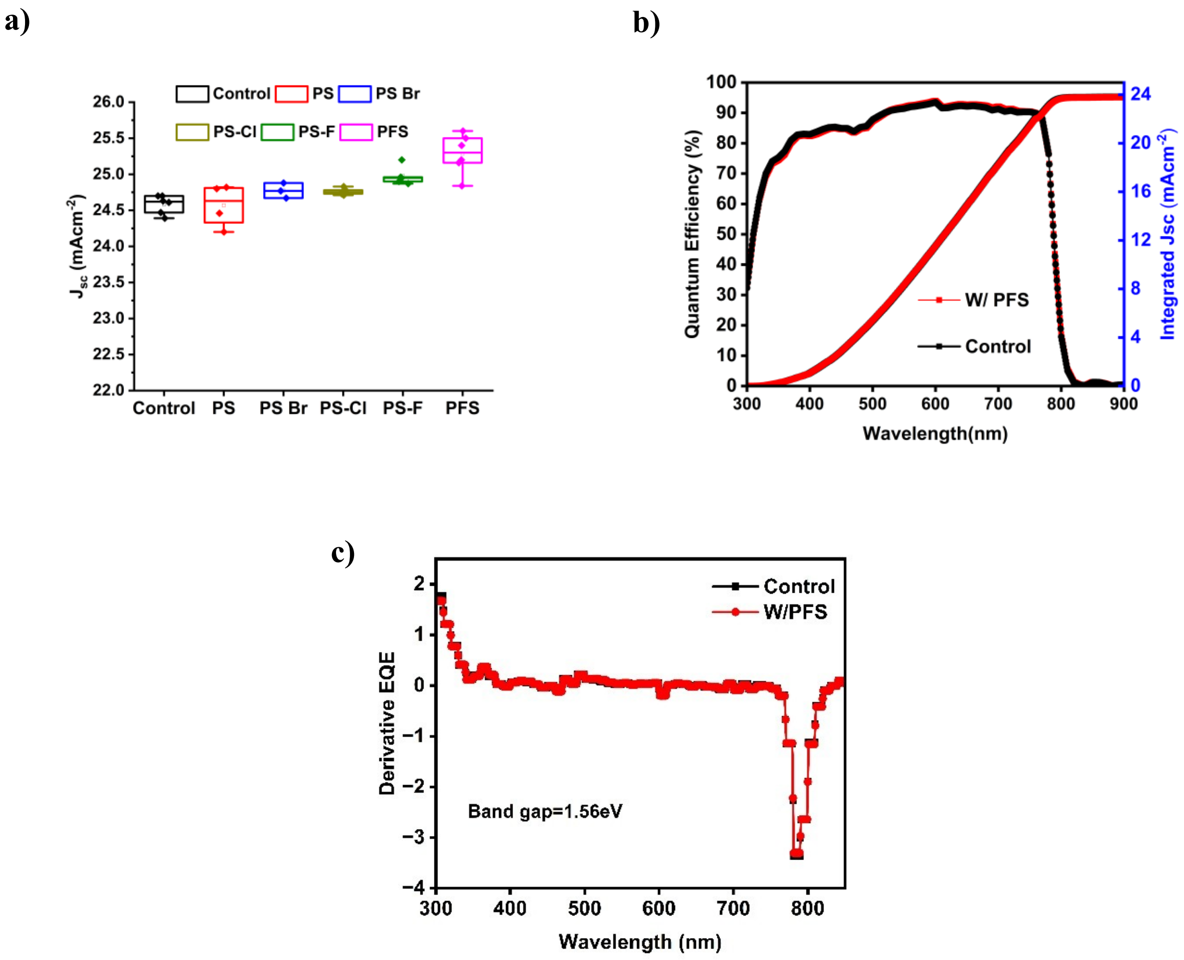

Fig S21 a) Box plot of Jsc for multiple control, PS, PS-Br, PS-Cl, PS-F and PFS incorporated perovskite thin films. **b)** EQE and integrated J_{sc} for control and PFS modified perovskite thin films. **c)** Band gap of perovskite determined form the derivative of EQE spectrum.

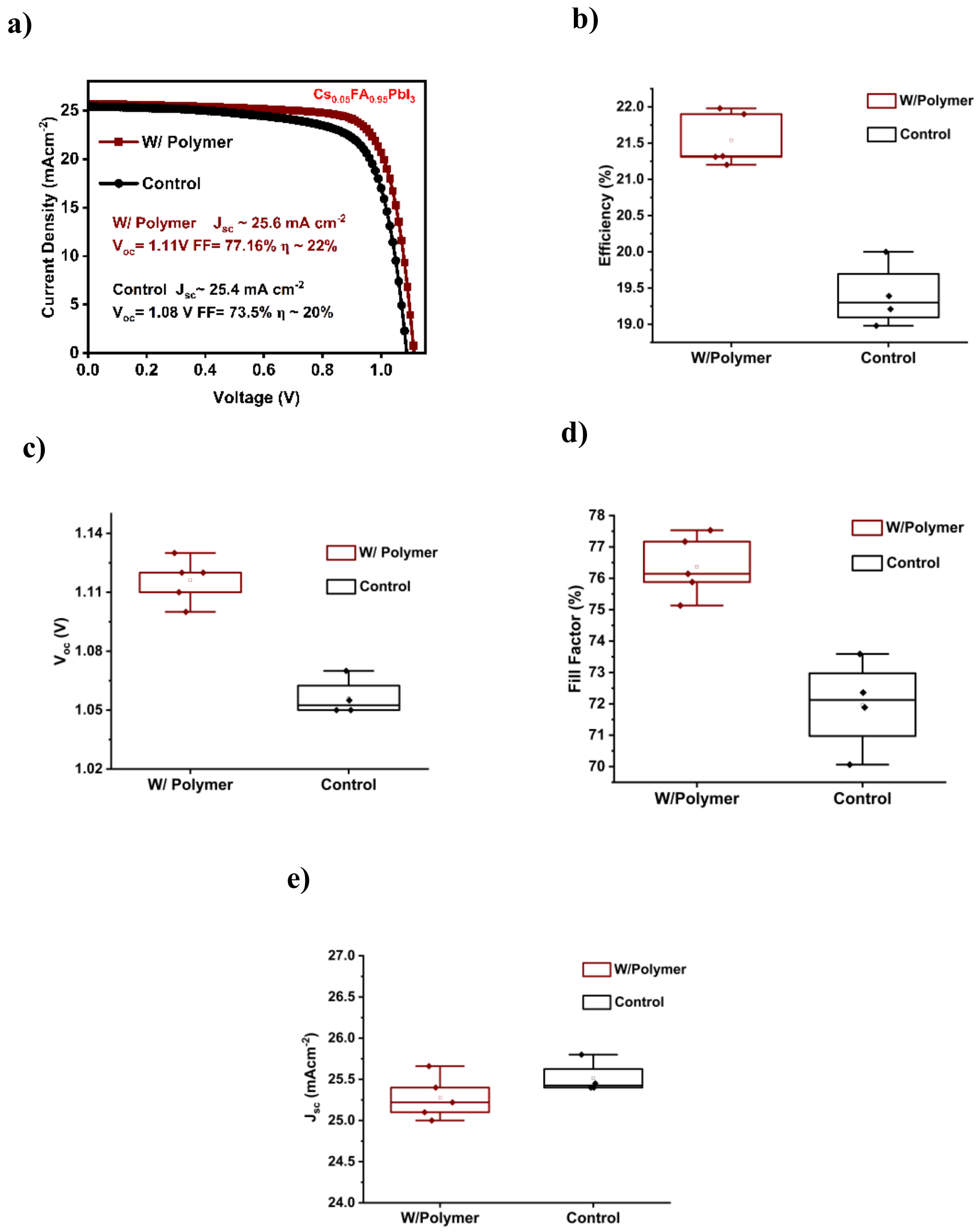

Fig S22. a) Champion J-V curves for control and PFS passivated perovskite solar cells based on $Cs_{0.05}FA_{0.95}PbI_3$ composition. Box plot for **b)** Efficiency **c)** V_{oc} **d)** Fill factor **e)** J_{sc} for multiple or control and PFS passivated perovskite devices

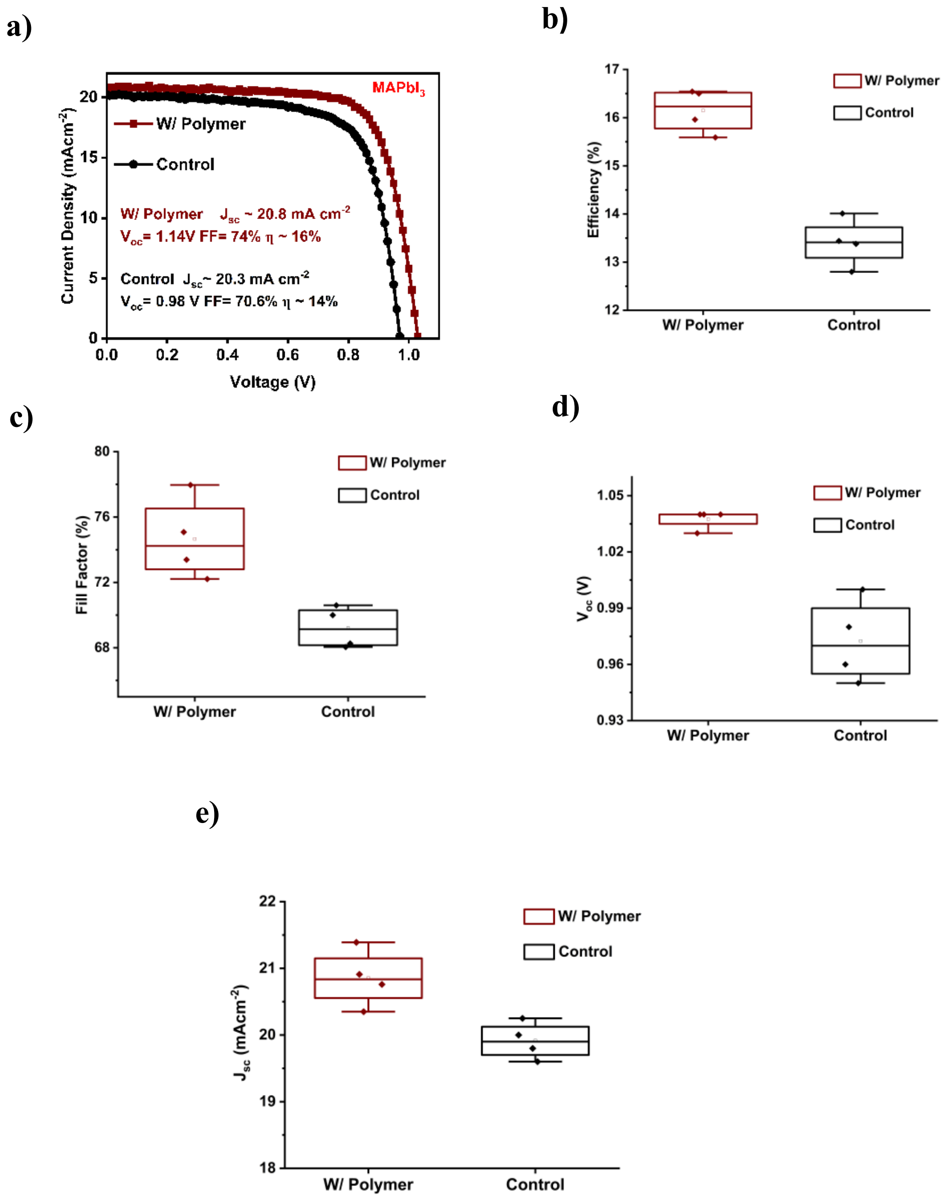

Fig S23. a) Champion J-V curves for control and PFS passivated perovskite solar cells based on $MAPbI_3$ composition. Box plot for **b)** Efficiency **c)** V_{oc} **d)** Fill factor **e)** J_{sc} for multiple or control and PFS passivated perovskite device

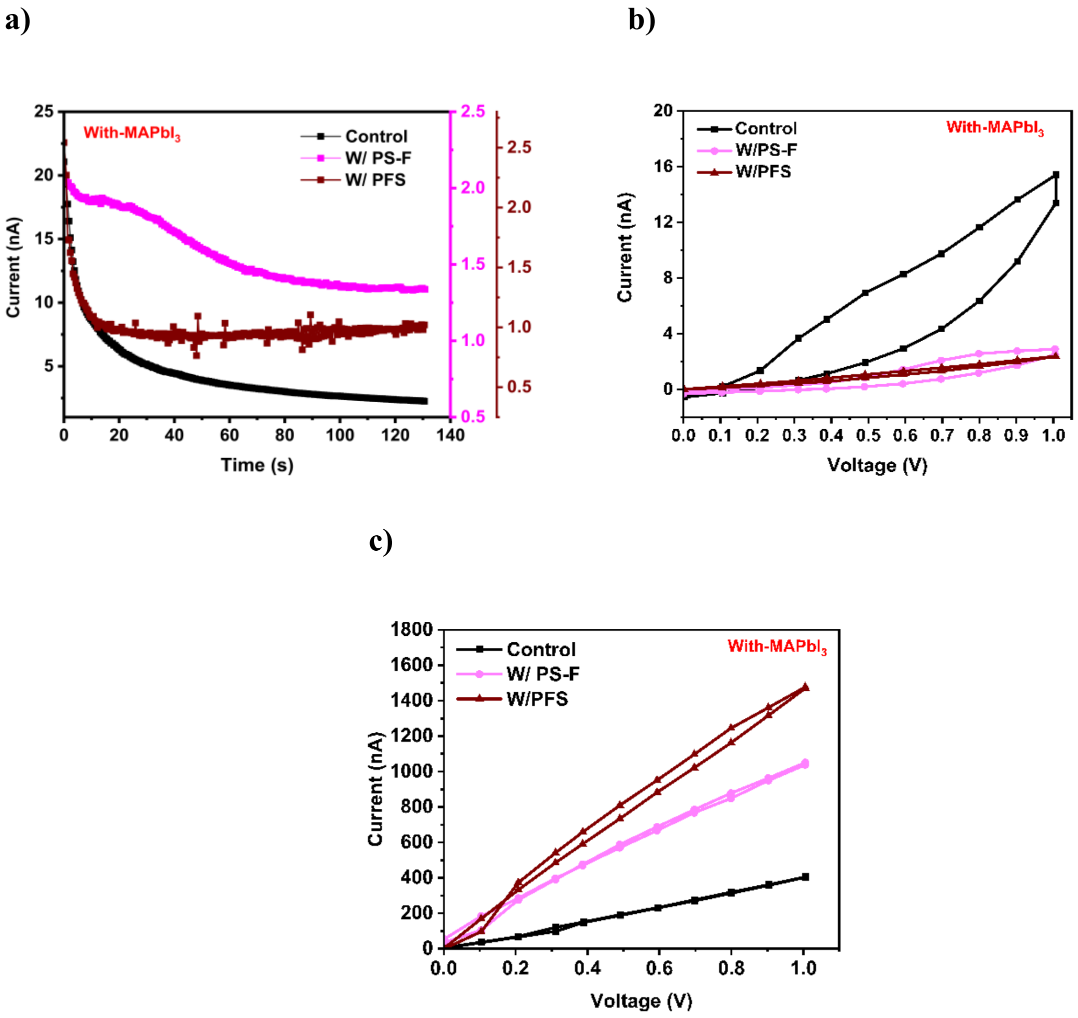

Fig S24. **a)** Dark poling curves at 1V of constant DC bias **b)** Dark I-V **c)** I-V in light for control, PS-F and PFS passivated MAPbI$_3$ perovskite thin film.

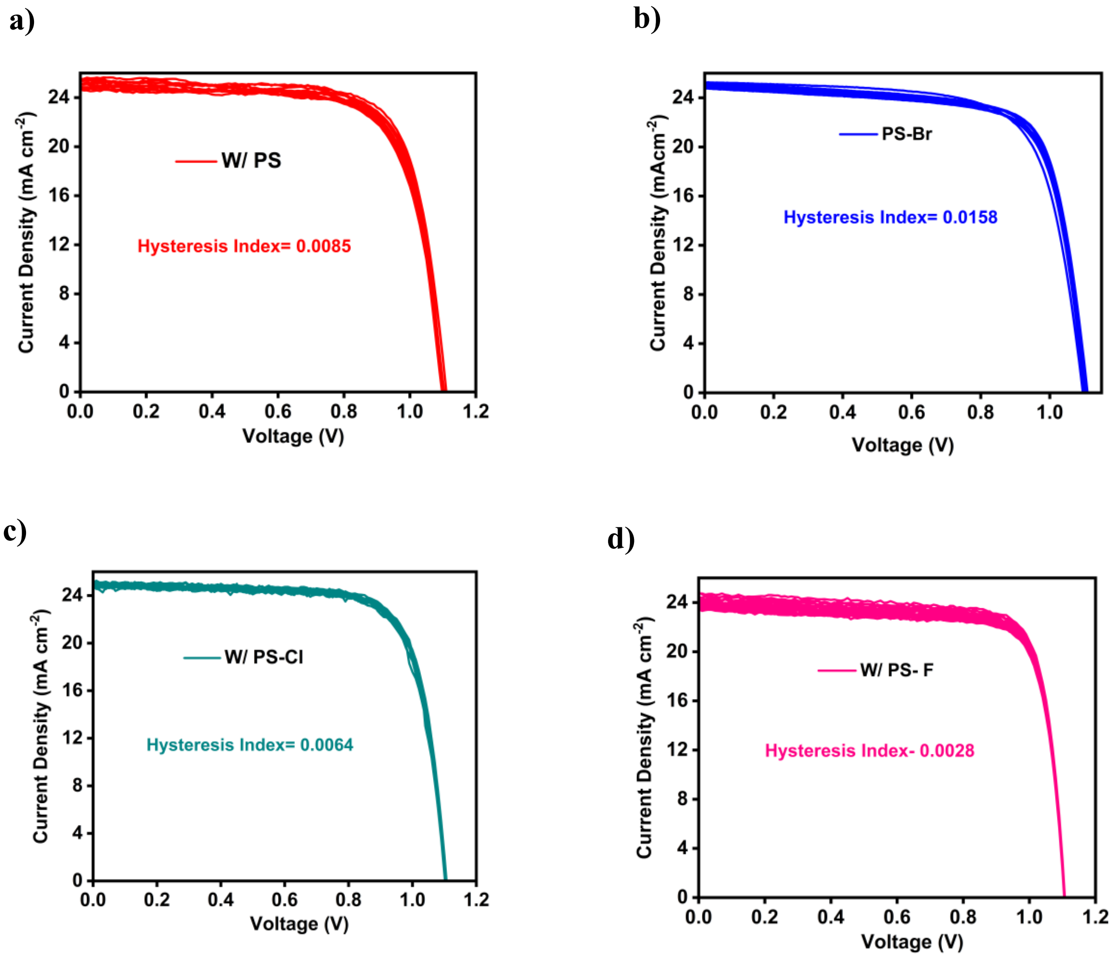

Fig S25 a, b, c, d) Ten continuous J-V hysteresis curve for PS, PS-Br, PS-Cl, PS-F polymer incorporated perovskite thin films with their corresponding hysteresis index.

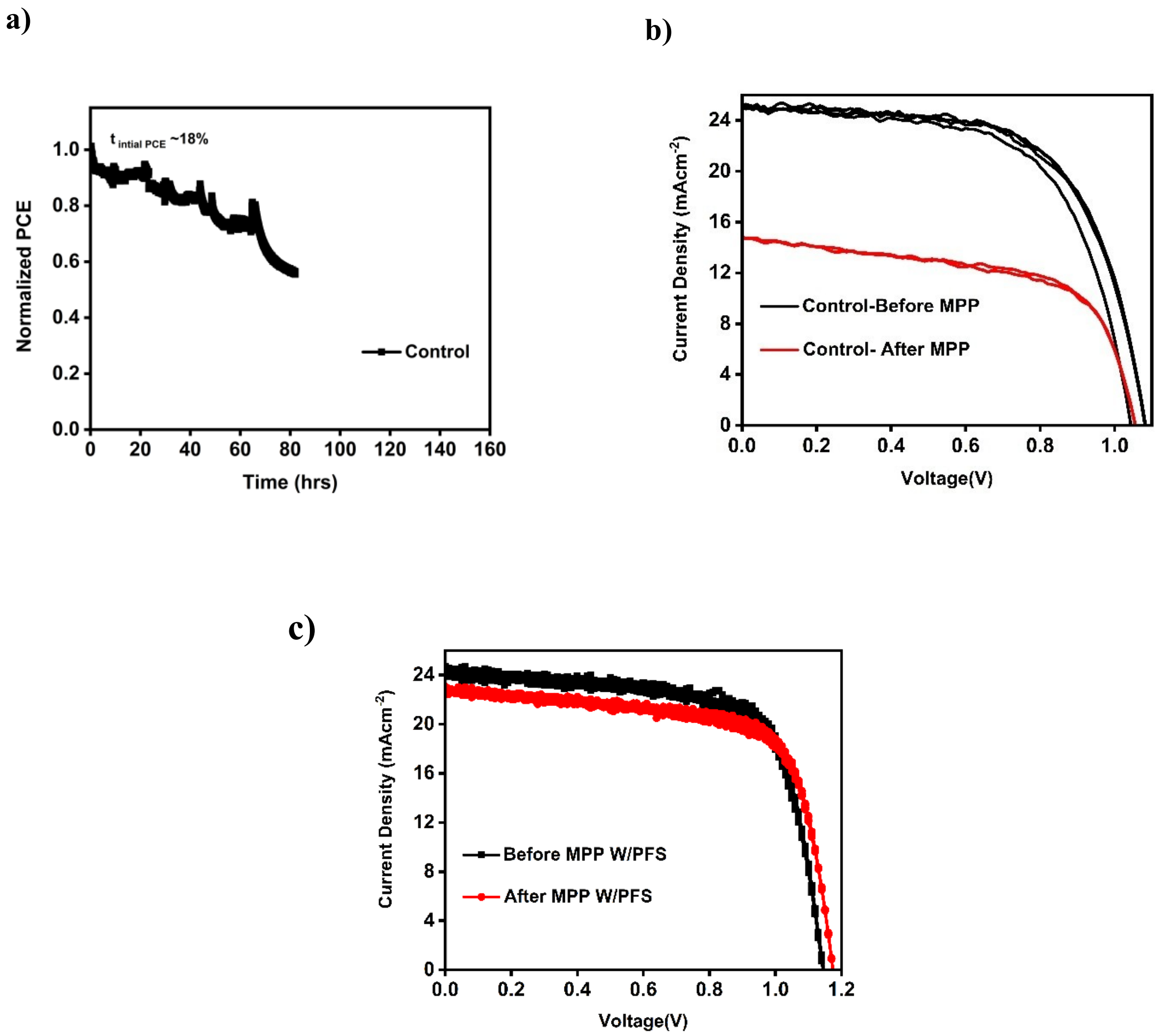

Fig S26 a) MPP tracking for control perovskite solar cells uner ISOS-L1 conditions **b, c)** J-V scans for control and PFS polymer incorporated perovskite devices before and after MPP tracking.

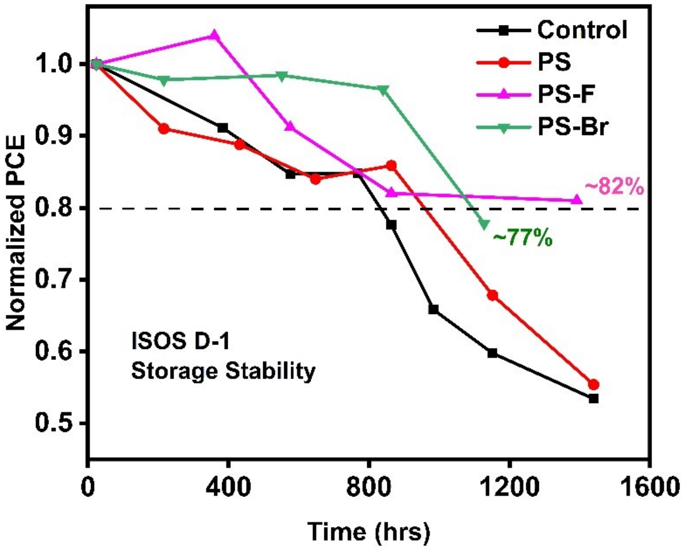

Fig S27 ISOS D-1 storage stability for control PS, PS-Br and PS-F modified perovskite thin films under ambient conditions (RH 40±20% at room temperature).

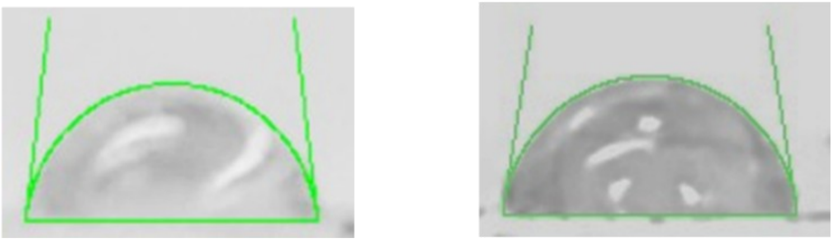

W/PS-Cl - 81° **W/PS-Br - 83°**

Fig S28 Water contact angle for PS-Cl and PS-Br incorporated polymer-perovskite thin films

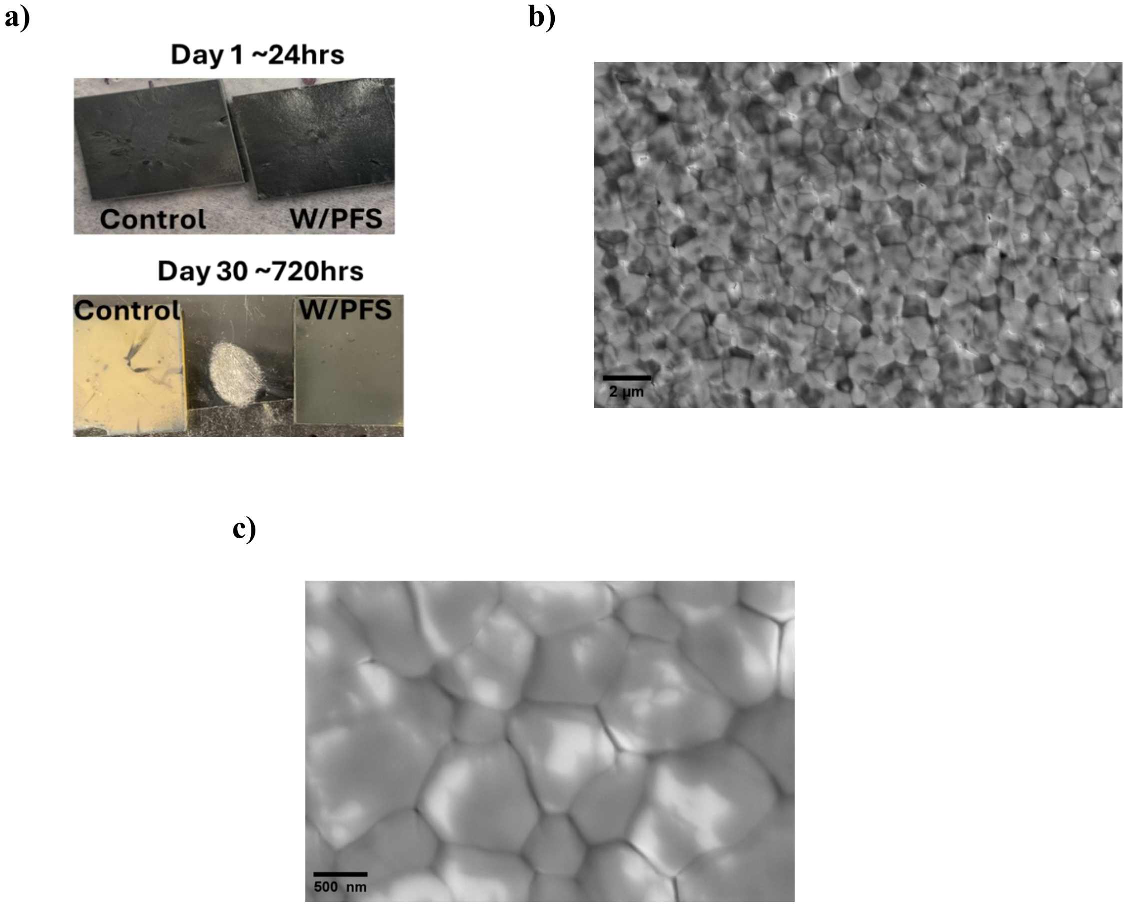

Fig S29 a) Photographs of control and PFS perovskite thin film stored under ambient conditions (RH 40±20% at room temperature) for 30 days. **b)** Top view SEM image of conformal polymer interlayer coated on perovskite thin film **c)** Zoom in SEM image of perovskite grain uniformly covered by a thin polymer layer. The white spots on the gains are formed due to the removal of polymer layer by the electron beam. The black covered region represents the uniform polymer coating.

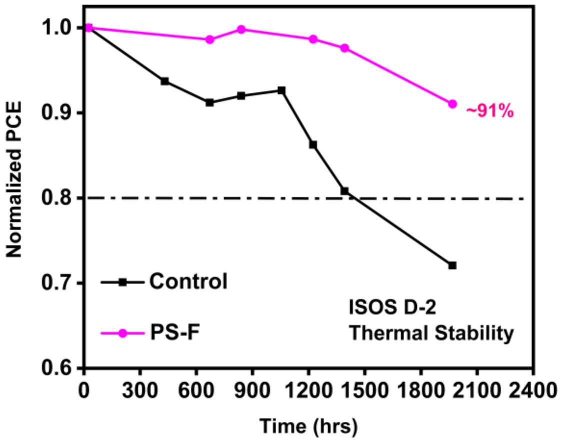

Fig S30 ISOS D-2 high-temperature thermal stability of control and PS-F modified perovskite thin films under high temperature (RH 40±20% at 65°C).

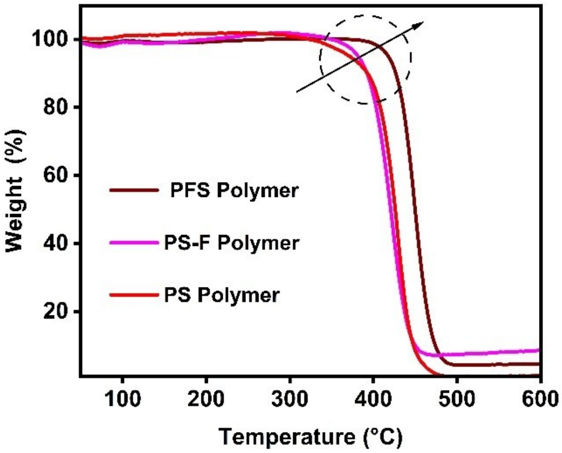

Fig S31 TGA weight loss curves for PFS, PS-F and PS polymer powders measured under inert (Ar) conditions. The circular dotted region with arrows signifies the improved thermal stability of PFS polymer when compared to PS and PS-F polymer.

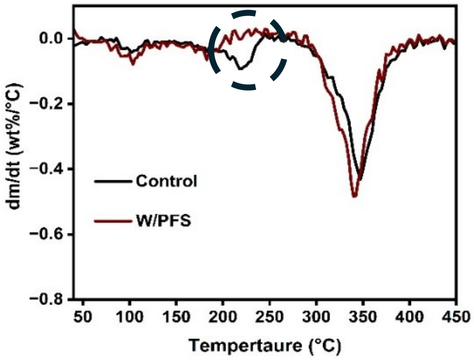

Fig S32 DTGA weight loss curves for control and PFS-modified perovskite powders measured under inert (Ar) conditions.

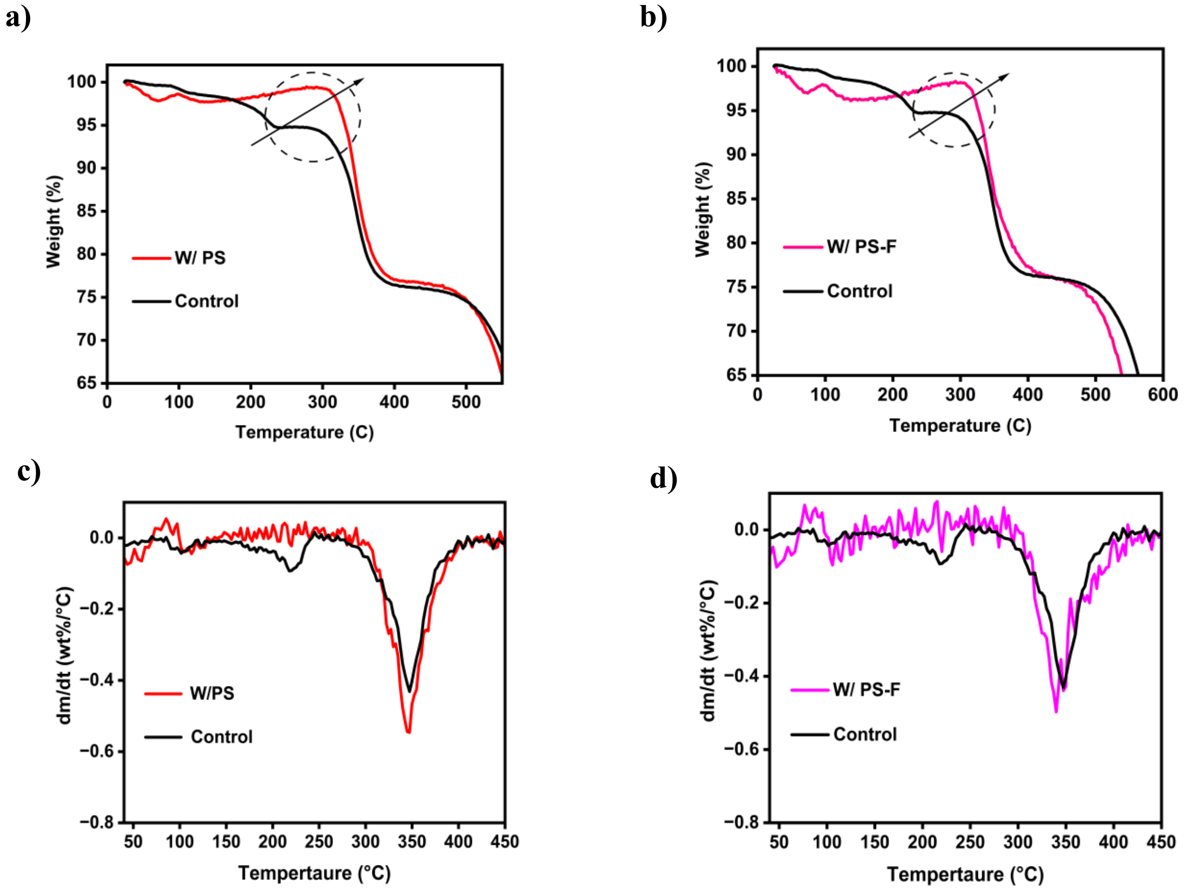

Fig S33 a, b) TGA weight loss curves for control, PS and PS-F modified perovskite powders measured under inert (Ar) conditions. The circular dotted region with arrows signifies the improved thermal stability of PS and PS-F -modified perovskite powders when compared to the control. **c, d)** DTGA weight loss curves for control PS, and PS-F-modified perovskite powders measured under inert (Ar) conditions

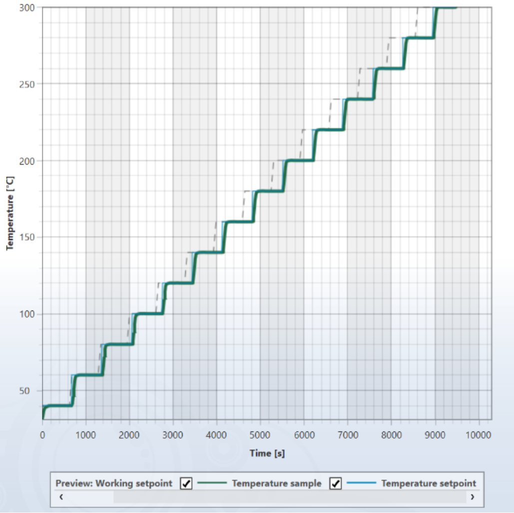

Fig S34 Photograph of heating temperature profile that was used for high temperature XRD analysis of control and PFS modified perovskite thin films.

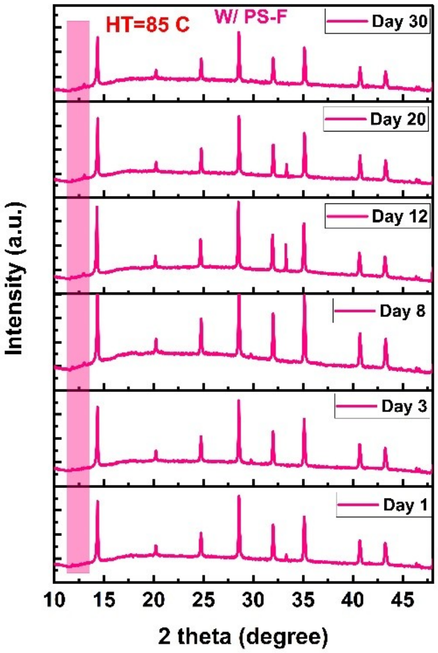

Fig S35 XRD diffraction patterns taken at regular time intervals for PS-F modified perovskite thin films stored under high temperature of 85°C and RH of 40±20%.

Table S1. Summary of Band gap, Valence band edge, conduction band edge and work function.

Sample	**Band gap (eV)**	**Valence Band (eV)**	**Conduction band (eV)**	**Work function (eV)**
Control	1.56	-5.22	-3.66	4.19
PS	1.56	-5.28	-3.72	4.62
PS-Br	1.56	-5.52	-3.96	4.67
PS-Cl	1.56	-5.55	-3.99	4.82
PS-F	1.56	-5.57	-4.01	4.86
PSF	1.56	-5.68	-4.12	4.88
C60	1.68	-5.91	-4.23	4.36

Table S2. Dipole moment of different halogenated monomers.

Monomer	**x**	**y**	**z**	**Dipole (D)**	**Quadrupole moment (ZZ)**
Styrene	0.044	0.058	0	0.184987592	-6.1439
4Bromostyrene	0.2749	0.6121	0	1.705002328	-5.9335
4chlorostyrene	0.291	0.6499	0	1.80938294	-4.7411
4fluorostyrene	0.1674	0.40694	0	1.11810619	-4.1162
Pentafluoro styrene	0.289	0.5285	0	1.530587649	1.2655

Table S3. Summarized photovoltaic parameters of champion devices with their hysteresis indexes.

Sample	**Efficiency (%)**	**Jsc (mAcm^{-2})**	**Voc (V)**	**FF (%)**	**HI**
W/PFS	24	25.4	1.16	81.4	0.003
W/PS-F	22.5	25.2	1.14	78	0.0028
W/PS-Cl	21.14	24.75	1.11	76.7	0.0064
W/PS-Br	20.64	24.67	1.1	76	0.0158
W/PS	20	24.8	1.09	74	0.0085
Control	19.7	24.8	1.08	73.5	0.073